Int. J. Solids Structures, 1967, Vol. 3, pp. 293 to 308. Pergamon Press Ltd. Printed in Great Britain

OBSERVATIONS OF STRESS WAVE PROPAGATION IN A HALF-PLANE WITH BOUNDARY LOADING

J. W. DALLY and S. A. THAU

Department of Mechanics, Illinois Institute of Technology

Abstract—This investigation treats the half-plane with a boundary load using a combined theoretical and experimental analysis. The theoretical approach considers an isotropic, perfectly elastic, semi-infinite plate with a concentrated normal load on the boundary. The experimental model consisted of a large sheet of columbia resin CR-39 loaded with a charge of lead azide in a semi-cylindrical pit on the edge of the plate. Results for the boundary stress from the theoretical and dynamic photoelastic analyses were compared. The comparison showed agreement for effects due to the *P* wave and marked but explainable differences in the theoretical and experimental results associated with the *S* and *R* waves. It appears that a better correlation between loading functions for the experimental and mathematical models is required in order to improve agreement.

1. INTRODUCTION

THE analysis of the response of a dynamically loaded elastic half-plane is of interest in both the application and the theory of elastic wave propagation. When the thickness of the plane is small compared to the characteristic wave lengths of the disturbance, the half-plane serves as a two-dimensional generalized plane stress model for studying the transmission of stress waves along a free boundary, such as the surface of the earth [1]. In addition, the phenomenon of the coupling along the free boundary of the dilatational and shear waves, the generation of the von Schmidt wave at the boundary, plus the existence of a distinct boundary wave, i.e. the familiar Rayleigh wave, are all described in the dynamic half-plane problem.

The characteristics of wave propagation in a half-plane with a concentrated force acting on the boundary and a half-space with a concentrated line load on the surface are equivalent. Solutions for this problem are presented by Sherwood [2] and Fung [3] when the time dependence of the load is a step function or a delta function. However, neither of these functions represent loadings that can be imposed on the model in the laboratory. Furthermore, solutions obtained with the step or delta functions predict infinite Rayleigh stress wave amplitudes along the free edge. In this study, a triangular pulse with finite rise and decay times was selected as the loading function which represented a first approximation to explosively induced loads applied in the associated experimental investigation.

Various aspects of the half-plane problem have been examined by employing dynamic photoelasticity by Feder *et al.* [4] and Dally *et al.* [5]. Dynamic photoelasticity is particularly suited for an experimental investigation of the half-plane since it yields full field results. If the experimental model is sufficiently large and the loading time is sufficiently short, the four stress waves (dilatational, shear, von Schmidt and Rayleigh) separate and their individual characteristics can be examined.

The present investigation treats the half-plane with a boundary load using a combined theoretical and experimental analysis. Experimental and theoretical results for the principal stresses along the free edge of the half-plane are obtained and compared. Also, the decay

rates of the maximum compressive and tensile stress amplitudes of the dilatational wave are compared. These comparisons show many similarities between the theoretical and experimental results; however, striking differences which exist in regard to the Rayleigh wave amplitudes indicate that the experimental and theoretical models are not perfectly matched. Photoelastic results for the Rayleigh wave are presented which indicate its influence extends a distance below the boundary which is about 0·35 to 0·40 of its distance from the load.

2. THEORETICAL DESCRIPTION OF WAVES IN A HALF-PLANE

2.1 *Definition of problem*

For a mathematical description of the dynamic field in the half-plane with boundary loading which is observed by the photoelastic method, an isotropic, perfectly elastic, semi-infinite plate with a concentrated normal load was considered. A Cartesian coordinate system was chosen with the y-axis acting in the direction of loading and the x–y plane coinciding with the median plane of the plate as shown in Fig. 1.

It was assumed further that the thickness dimension of the half-plane, measured along the z direction, was smaller than the predominant wave lengths of the disturbance; i.e. a two-dimensional, generalized plane stress analysis was employed where the elastodynamic field quantities were averaged across the thickness of the plate. For example, the average displacement in the x-direction, $u(x, y, t)$, is given by

$$u(x, y, t) = (2b)^{-1}\int_{-b}^{b} \bar{u}(x, y, z, t)\,dz \tag{1}$$

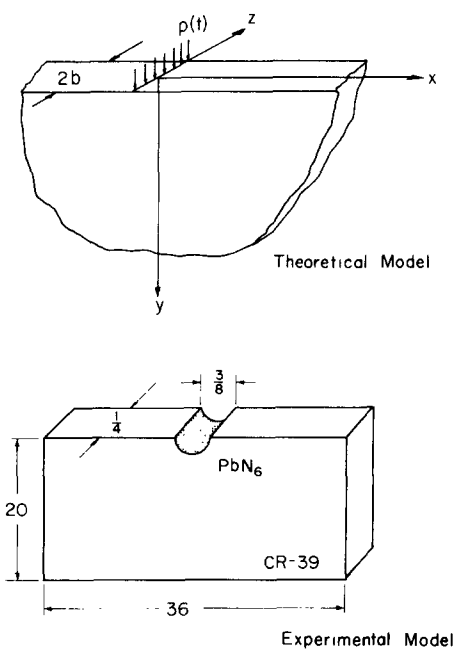

FIG. 1. Theoretical and experimental models.

where $2b$ is the thickness of the plane and $\bar{u}$ is the actual three-dimensional x-component of displacement. With similar equations for the average y displacement, $v(x, y, t)$, and the average stresses, $\tau_{ij}(x, y, t)$, the boundary conditions along the surfaces of the plate ($z = \pm b$) were satisfied by setting τ_{xz}, τ_{yz}, and τ_{zz} equal to zero.

Hooke's Law, relating the stresses and displacement gradients for the generalized plane stress state becomes:

$$\begin{aligned}
\tau_{xx} &= 2\mu\left[\frac{\partial u}{\partial x}+\frac{\nu}{1-\nu}\left(\frac{\partial u}{\partial x}+\frac{\partial v}{\partial y}\right)\right] \\
\tau_{yy} &= 2\mu\left[\frac{\partial v}{\partial y}+\frac{\nu}{1-\nu}\left(\frac{\partial u}{\partial x}+\frac{\partial v}{\partial y}\right)\right] \\
\tau_{xy} &= \mu\left[\frac{\partial u}{\partial y}+\frac{\partial v}{\partial x}\right] \\
\tau_{xz} &= \tau_{yz} = \tau_{zz} = 0
\end{aligned} \tag{2}$$

where μ and ν are the shear modulus and Poisson's ratio of the material, respectively. The z-displacement is related to the average x and y displacement components by

$$\bar{w}(x, y, z, t) = -\nu z(\partial u/\partial x+\partial v/\partial y)/(1-\nu). \tag{3}$$

Introducing the wave potentials [1], $\varphi(x, y, t)$ and $\psi(x, y, t)$, as

$$u = \partial\varphi/\partial x+\partial\psi/\partial y, \qquad v = \partial\varphi/\partial y-\partial\psi/\partial x \tag{4}$$

one may write the equations of motion as:

$$(c_1^2\nabla^2-\partial^2/\partial t^2)\varphi = 0, \qquad (c_2^2\nabla^2-\partial^2/\partial t^2)\psi = 0 \tag{5}$$

where ∇^2 is the two-dimensional Laplacian operator and the wave velocities, c_1 and c_2, defined by

$$c_1 = \kappa c_2, \qquad c_2 = (\mu/\rho)^{\frac{1}{2}}, \qquad \kappa^2 = 2/(1-\nu) \tag{6}$$

characterize the dilatational or P waves ($\varphi(x, y, t)$) and the shear or S waves ($\psi(x, y, t)$), respectively. Since $\kappa > 1$, the P wave travels with the greater velocity. Note from (2), (4), (5), and (6) that

$$\tau_{xx}+\tau_{yy} = (1+\nu)(\mu/c_2^2)\partial^2\varphi/\partial t^2. \tag{7}$$

In the problem at hand for the semi-infinite plate occupying the region, $-\infty < x < \infty$, $0 \le y < \infty$, $|z| \le b$, the boundary conditions along $y = 0$ become

$$\tau_{xy}(x, 0, t) = 0, \qquad \tau_{yy}(x, 0, t) = -p(t)\,\delta(x) \tag{8}$$

where $\delta(x)$ is the Dirac delta function representing the concentrated vertical line load at $x = y = 0$ which extends across the thickness from $z = -b$ to $z = b$. The magnitude of the load, $p(t)$, will be chosen later to approximate the lead azide explosion in the experiment.

2.2 *Solution of problem*

Equations (2) through (8) along with the condition of outgoing radiation at infinity completely define the problem. The exact solution for certain basic loading functions, $p(t)$,

is known from [2] and [3] and thus, by the principle of superposition, solutions for arbitrary loading can be obtained.

The method for solving the problem which was followed is described in detail in Fung's text [3]. It involves transform techniques and contour integration. Since the main interest, however, is in evaluating the non-zero principal stress component τ_{xx} along the free edge of the plane ($y = 0$), only this result is given here. From equations (7) and (8) we have,

$$\tau_{xx}(x, 0, t) = [p(t)\,\delta(x) + (1+\nu)(\mu/c_2^2)\partial^2\varphi/\partial t^2]_{y=0}. \tag{9}$$

The first term on the right side of (9) is infinite at $x = 0$, but vanishes for all $x \neq 0$. This infinite stress value at $x = 0$ occurs because the concentrated force acts there. However, along the free edge away from the load, the stress depends on the second term in (9) alone. The final result is presented below with Poisson's ratio taken as $\nu = 1/3$ which is close to the value obtained experimentally for the CR-39 plate.

$$\tau_{xx}(x, 0, t) = \frac{2}{3\pi c_2}\left[-\int_{3^{-1/2}}^{1} f(\eta)\dot{p}\left(t - \frac{\eta x}{c_2}\right)d\eta + \frac{\pi c_2}{2c_R}\dot{p}\left(t - \frac{x}{c_R}\right)\right]; \qquad (x > 0) \tag{10}$$

where

$$f(\eta) = \frac{3\eta^2(\frac{1}{2} - \eta^2)[(1-\eta^2)(\eta^2 - \frac{1}{3})]^{\frac{1}{2}}}{2(\eta^2 - \frac{1}{4})\left(\eta^2 - \dfrac{3-3^{\frac{1}{2}}}{4}\right)\left(\dfrac{3+3^{\frac{1}{2}}}{4} - \eta^2\right)} \tag{11}$$

and the Rayleigh wave velocity, c_R, is given by

$$c_R = 2c_2/(3+3^{\frac{1}{2}})^{\frac{1}{2}} \approx 0{\cdot}92\,c_2$$

and $\dot{p}$ indicates dp/dt. The results for $x < 0$ can be obtained from (10) by symmetry.

To interpret the solution, note first that in an actual situation the loading begins at $t = 0$, i.e.

$$p(t) = \dot{p}(t) = 0 \quad \text{for} \quad t \leq 0.$$

Hence, if the value of observation time is fixed at $t = \bar{t}$, say, ($\bar{t} > 0$), we obtain from (10),

$$\tau_{xx}(x, 0, \bar{t}) = 0; \qquad c_1\bar{t} = 3^{\frac{1}{2}}c_2\bar{t} \leq x \tag{12a}$$

$$\tau_{xx}(x, 0, \bar{t}) = -\frac{2}{3\pi c_2}\int_{3^{-1/2}}^{c_2\bar{t}/x} f(\eta)\dot{p}\left(\bar{t} - \frac{\eta x}{c_2}\right)d\eta; \qquad c_2\bar{t} \leq x \leq c_1\bar{t} \tag{12b}$$

$$\tau_{xx}(x, 0, \bar{t}) = -\frac{2}{3\pi c_2}\int_{3^{-1/2}}^{1} f(\eta)\dot{p}\left(\bar{t} - \frac{\eta x}{c_2}\right)d\eta; \qquad c_R\bar{t} \leq x \leq c_2\bar{t} \tag{12c}$$

$$\tau_{xx}(x, 0, t) = \frac{2}{3\pi c_2}\left[-\int_{3^{-1/2}}^{1} f(\eta)\dot{p}\left(\bar{t} - \frac{\eta x}{c_2}\right)d\eta + \frac{\pi c_2}{2c_R}\dot{p}\left(\bar{t} - \frac{x}{c_R}\right)\right]; \qquad 0 < x \leq c_R\bar{t}. \tag{12d}$$

Thus, it can be seen that before the P wave arrives, equation (12a), there is no response. From the leading front of the S wave to the leading front of the P wave the stress is expressed

by (12b). The stress associated with the S wave from the leading front of the Rayleigh wave to the leading front of the S wave is in (12c) while the arrival of the Rayleigh wave and the stress distribution from the loading point up to the Rayleigh wave is denoted by (12d). The solution then indicates the effects of three distinct waves*, P, S, and Rayleigh, traveling along the surface. The P wave velocity for $\nu = \frac{1}{3}$ is, $c_1 \approx 1{\cdot}73\, c_2$, and, as given above, the Rayleigh wave moves with the smallest velocity, $c_R \approx 0{\cdot}92\, c_2$.

Of interest is the fact that the Rayleigh wave amplitude is directly proportional to the rate of loading. The P and S waves, however, are less sensitive to the loading rate since they are associated with the integrals in equations (12) which "smooth out" the loading function.

2.3 *Properties of the Rayleigh wave for pulse loading*

Further details of the stress response along the free edge of the half-plane (equations 12) can be observed after the time dependence of the load, $p(t)$ is specified. Although the exact form for this function in the experiment cannot be determined, a reasonable approximation for it is the triangular pulse shown in Fig. 2. Mathematically, this is expressed by

$$\begin{aligned} p(t) &= p_0 t/t_0; \qquad 0 < t < t_0 \\ p(t) &= p_0(t_1 - t)/(t_1 - t_0); \qquad t_0 < t < t_1 \\ p(t) &= 0; \qquad t_1 < t. \end{aligned} \tag{13}$$

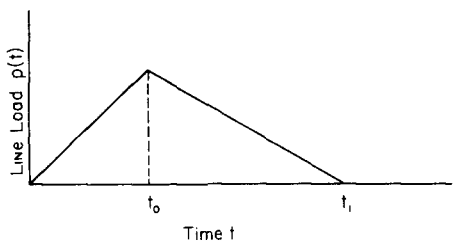

FIG. 2. Loading function.

In (13), p_0 is the peak value of the load, t_0 is the rise time, and t_1 is the total pulse duration time. Thus, $t_1 - t_0$ is the decay time of the load.

By differentiating the above relations we obtain

$$\begin{aligned} \dot{p}(t) &= p_0/t_0; \qquad 0 < t < t_0 \\ \dot{p}(t) &= -p_0/t_0[t_0/(t_1 - t_0)]; \qquad t_0 < t < t_1 \\ \dot{p}(t) &= 0; \qquad t_1 < t \end{aligned} \tag{14}$$

which indicate constant rates of loading and unloading. The ratio of the rate of unloading to the rate of loading is $t_0/(t_1 - t_0)$ = rise time/decay time.

Values of t_0 and t_1 for numerical calculation are chosen from certain characteristics of the experimental results which will be discussed below. For the following analysis, it is

* On the boundary the P wave and von Schmidt wave are superimposed and their individual features cannot be distinguished (see Fig. 6). Their combined effect is treated here as a P wave.

pointed out that $(t_1 - t_0) > t_0$ and the time is taken as $t = \bar{t} > t_1$, i.e. the response at fixed times after the load has been completely removed is discussed.

Because of its simple form, the Rayleigh wave, which arrives at the position, $x = c_R\bar{t}$, can be analyzed in some detail. From (12d) and (14) one obtains:

$$\begin{aligned} \tau_{xx}]_R &= p_0/3c_Rt_0; \qquad c_R(\bar{t}-t_0) < x < c_R\bar{t} \\ \tau_{xx}]_R &= -(p_0/3c_Rt_0)[t_0/(t_1-t_0)]; \qquad c_R(\bar{t}-t_1) < x < c_R(\bar{t}-t_0) \end{aligned} \tag{15}$$

and for $x < c_R(\bar{t}-t_1)$ the Rayleigh wave disturbance vanishes. Therefore, the Rayleigh wave propagates along the boundary in the form of two rectangular pulses. The leading pulse produces a tensile stress of magnitude, $p_0/3c_Rt_0$, and extends a distance c_Rt_0. The second pulse is compressive, with a magnitude $p_0/3c_R(t_1-t_0)$ and width $c_R(t_1-t_0)$. It is noted that the areas of the two pulses are equal which yields the following relation

$$\frac{\text{magnitude of tensile pulse}}{\text{magnitude of compressive pulse}} = \frac{\text{width of compressive pulse}}{\text{width of tensile pulse}} \tag{16}$$

Furthermore, since the ratio of the width of the tensile pulse to that of the compressive pulse is equal to (rise time)/(decay time) one obtains

$$\frac{\text{magnitude of tensile pulse}}{\text{magnitude of compressive pulse}} = \frac{\text{rise time of load}}{\text{fall time of load}} \tag{17}$$

This relation was used to calculate the ratio of rise time to fall time from the experimentally determined ratio of the magnitude of the Rayleigh tensile peak to the compressive peak.

The theoretical prediction that the Rayleigh wave suddenly rises, reverses its magnitude, and then decays, occurs from the choice of the loading function. For any loading, however, the Rayleigh wave at the free boundary exhibits stresses given by:

$$\tau_{xx}(x, 0, t)]_R = \dot{p}(t - x/c_R)/3c_R. \tag{18}$$

A description of the P and S wave contributions to the stress along the edge is more complicated, and is easier to discuss from the numerical results. This is done in a subsequent section. However, some features associated with the P wave arrival, which may be discerned directly from the analytical solution, are that the stress is initially compressive, reaching its peak compressive value at $x = c_1(\bar{t}-t_0)$ for $(\bar{t} > t_1)$; and that the stress then changes sign and reaches a tensile peak at about $x = c_1(\bar{t}-t_1)$. The point at which the initial compressive pulse ends depends on the relative values of t_0 and t_1.

By obtaining experimentally the distance from the leading front of the P wave to the point where the compressive peak occurs (equal to c_1t_0), the numerical value of t_0 was approximated. The value of t_1 was then established from equation (17) as indicated above.

3. DYNAMIC PHOTOELASTIC EXPERIMENT

3.1 *Description of experiment*

The experimental model of the half-plane was fabricated from a large sheet of columbia resin CR-39 to dimensions shown in Fig. 1. The sheet was sufficiently large to eliminate the

possibility of reflections from the boundaries during the time interval to separate the various stress waves.

Dynamic loading of the model was accomplished with a 250 mg charge of lead azide (PbN_6) packed into a semi-circular cavity at the top edge of the plate as illustrated in Fig. 1. The charge of lead azide was ignited at time $t = 0$ with a bridge wire detonator. The load intensity was sufficient to fracture the model in the local neighborhood about the cavity.

Dynamic isochromatic fringe patterns (light field) were recorded by employing a multiple spark Cranz–Schardin camera [6, 7] operating at an average framing rate of 65,000 fps. A total of 16 fringe patterns showing the photoelastic representation of the stress wave propagation over the time range from 60 to 290 μsec are presented in Fig. 3.

3.2 *Description of fringe patterns*

The formation of the fringe pattern changes markedly as the four stress waves propagate outward from the explosive source. An enlargement of frame 2 taken at $t = 66$ μsec, presented in Fig. 4, shows the P wave followed closely by the S wave. The von Schmidt (PS) wave is in its very early stage of development. The Rayleigh wave and the S wave are still superimposed at the boundary and their individual features cannot be distinguished.

An enlargement of frame 5 ($t = 107$ μsec) presented in Fig. 5 shows the four stress waves at various stages in their separation process. The P and S waves have completely separated and are quite distinct. The PS wave starting at the P front on the boundary and connecting to a tangent point on the S wave is becoming more evident. Near the boundary, the R and S waves are beginning to separate and the characteristic fringe pattern representing the R wave is observed.

The characteristics of the four stress waves are most clearly presented in Fig. 6 (enlargement of frame 10 at $t = 190$ μsec), when the separation of the waves is essentially complete. The leading P wave is shown by fringes which are nearly circular arcs with origins at the explosive source. The PS wave is represented by nearly plane fringes which make an angle of 35° with the boundary. The intersection of the PS wave with the shear wave yields a very complex fringe pattern in the region where the waves overlap. Two fringe peaks (N about 2·5) are separated by a narrow valley where the fringe order N is about zero. The fringes associated with the S wave follow the circular advancing front; however, due to the changing shear stress magnitude with angular position, the fringes are not circular arcs. The maximum shear stress occurs along a line making a 35° angle and decreases to relatively low values near the boundary and the vertical axis. The Rayleigh wave which closely follows the S front is a plane wave. On the boundary it exhibits a tensile peak followed by a compressive peak. Just below the boundary two isotropic points occur about in line with the boundary peaks. Between these isotropic points lies a fringe peak ($N = 3$). The fringe pattern associated with the Rayleigh wave indicates its plane front has traveled 7 in. and extends to a depth of about 2·5 in.

To further examine the depth of the Rayleigh wave disturbance reference is made to Fig. 7 where the fringe pattern corresponding to $t = 290\mu$ is shown. At this time, the plane front of the Rayleigh wave at a distance $x = 11$ in. is quite evident to a depth in the model of about 4 in. Thus, it appears that the Rayleigh wave cannot be considered as a localized boundary disturbance. While the boundary stresses are the most significant, the stresses at appreciable depths are by no means negligible.

4. THEORETICAL AND EXPERIMENTAL RESULTS

4.1 *Numerical data*

Measurements of the position of the P and R wave fronts and their corresponding times of arrival were made. Average velocities were then computed for c_1 and c_R as 72,000 and 38,200 in/sec respectively. The angle of the PS wave front with the edge of the model, θ, was established at 35° (see Fig. 6). The S wave velocity, c_2 was computed using this angle and the relation [1]:

$$c_2 = c_1 \sin\theta \tag{19}$$

to give $c_2 = 41{,}300$ in/sec.

The dynamic value of Poisson's ratio and the modulus of elasticity were computed from equation (6) using the previously established values of c_1 and c_2. Values of $\nu = 0{\cdot}34$ and $E = 559{,}000$ psi were obtained for the dynamic elastic constants (rate averaged) of CR-39.

Fringe order was established as a function of position along the boundary. The fringe orders were converted to principal stress by using the stress optic law:

$$\sigma_1 - \sigma_2 = \frac{N(f_\sigma)_d}{h}. \tag{20}$$

On the free boundary, equation (20) reduces to

$$\tau_{xx} = \frac{N(f_\sigma)_d}{h} \tag{21}$$

where N is the fringe order

h is the model thickness (0·262 in.)

$(f_\sigma)_d$ is the material fringe value 109 psi-in.

The material fringe value which was established by a static calibration was then corrected to a dynamic value of 109 psi-in following Clark's [8] calibration method.

Numerical results based on equations (12) and (14) for the principal stress, τ_{xx}, along the boundary were evaluated at observation times of 60, 92, 139 and 208 μsec which correspond to the photoelastic observations in frames 1, 4, 7 and 11. The integrations indicated in equation (12) were performed on the computer by a standard numerical procedure.

Rise and fall times for the ideal triangular pulse loading function (Fig. 2) were computed from the experimental data following the procedures previously discussed. However, a certain amount of spreading of the experimentally observed P wave compressive pulse occurs due to dispersion and dissipation. Hence, better agreement was obtained by choosing a value of rise time, t_0, less than that predicted by the measurement of the distance between the P wave front and the P wave compressive peak. The values selected were $t_0 = 9$ μsec, and, based on equation (17), $t_1 - t_0 = 11$ μsec.

The stresses given by equation (12) were normalized by the constant $\tau_0 = 2p_0/3\pi c_2 t_0$. Then the theoretical results so obtained were scaled by a factor of 24 which produced good agreement with the experimental results for the P wave tensile and compressive peaks at the intermediate observation time, $t = 92$ μsec.

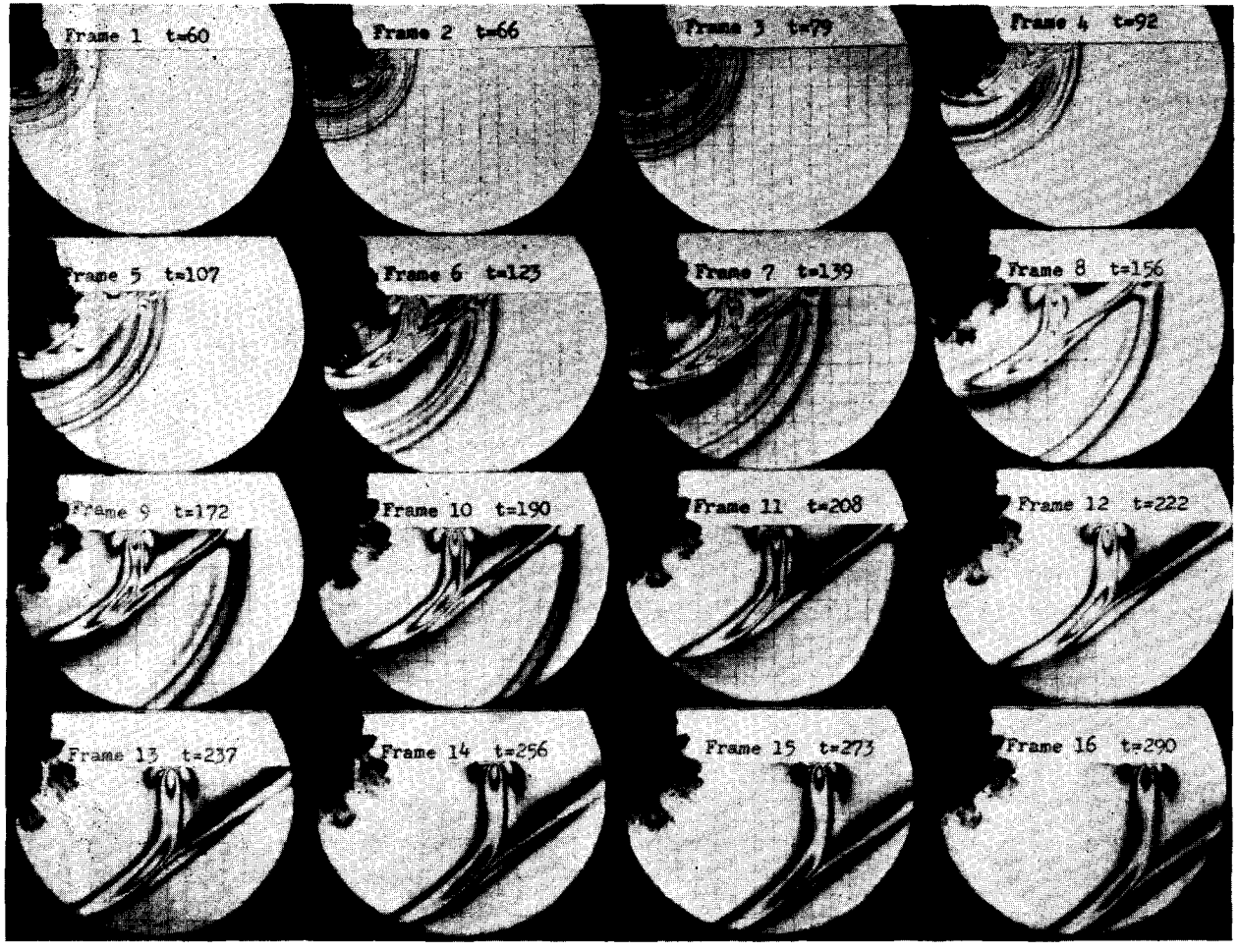

FIG. 3. Dynamic fringe patterns for a half-plane model with an explosive load supplied at the free surface (t in μsec and Cartesian grid on 1-in. centers).

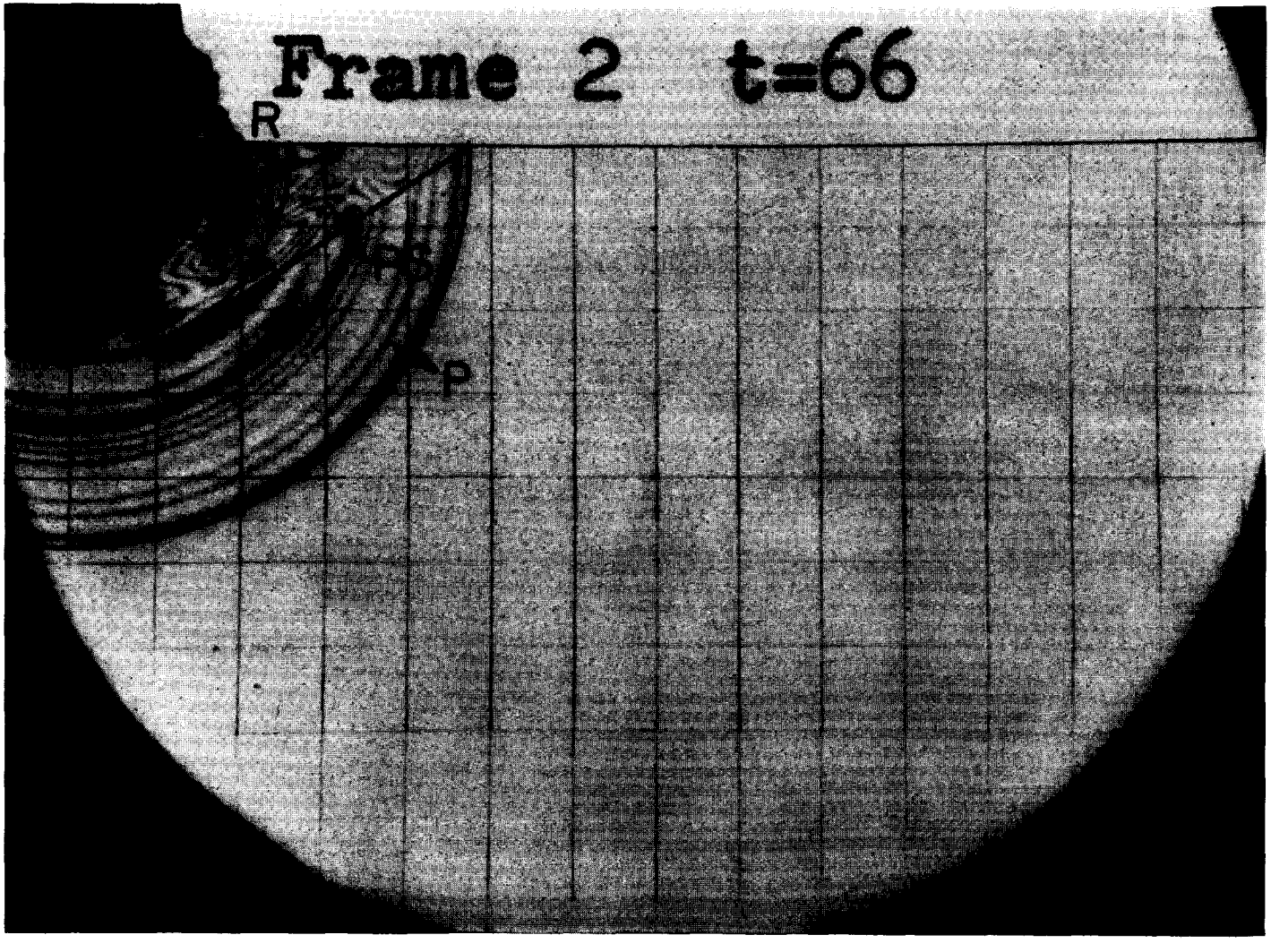

FIG. 4. Photoelastic representation of the four stress waves early in the dynamic event.

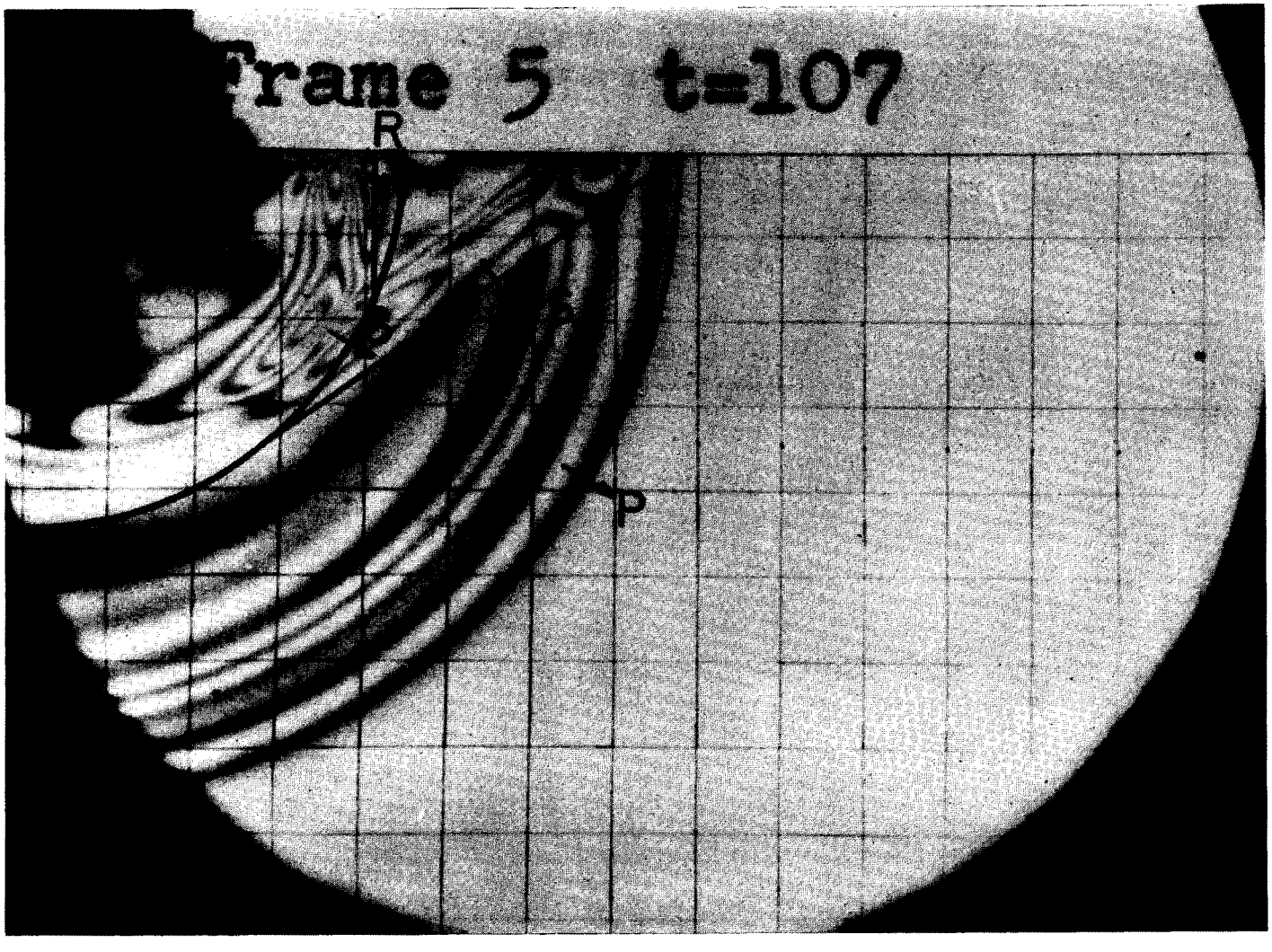

FIG. 5. Photoelastic representation of the stress waves at various stages of separation.

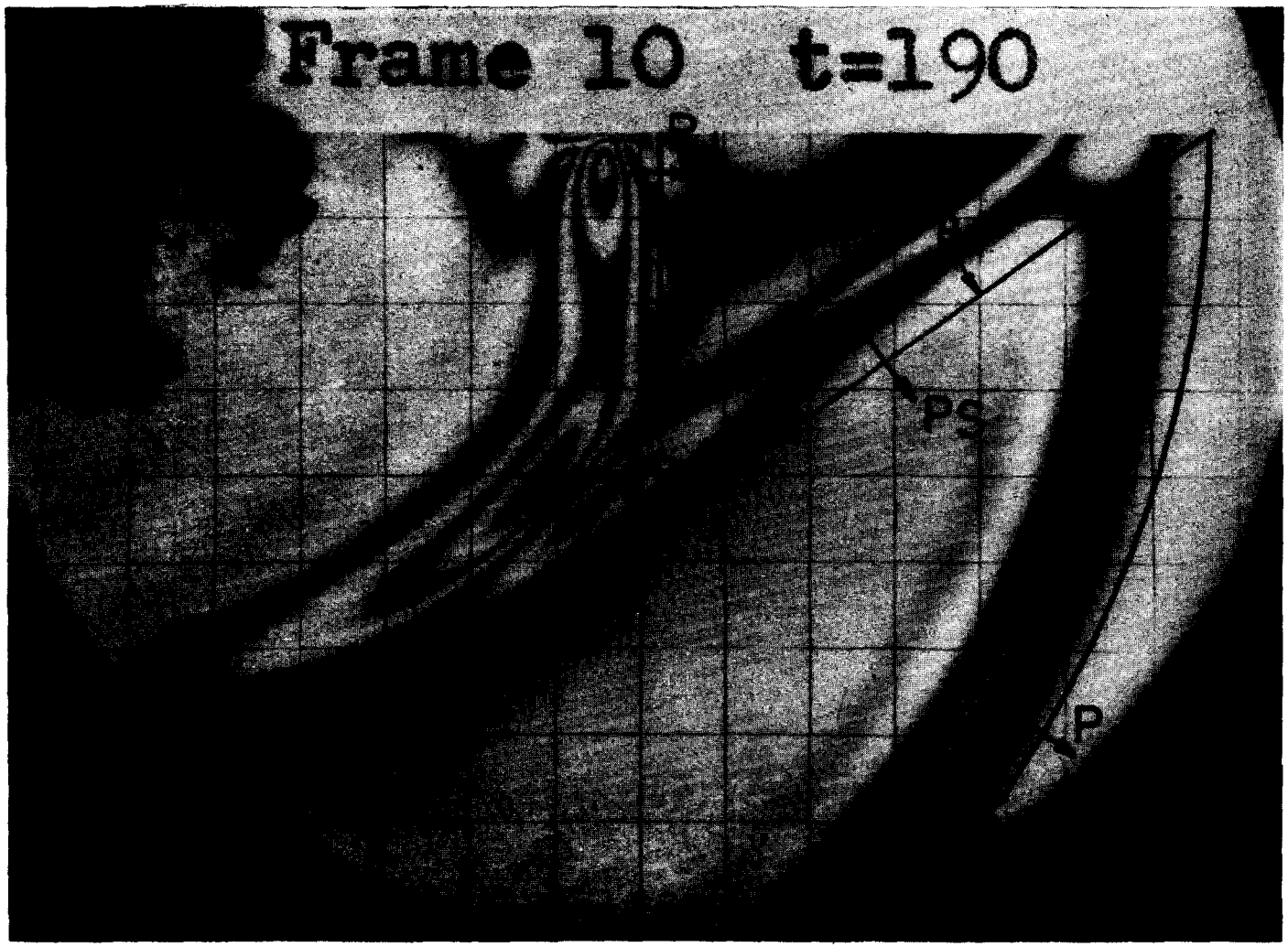

FIG. 6. Photoelastic representation of the four stress waves after separation is complete.

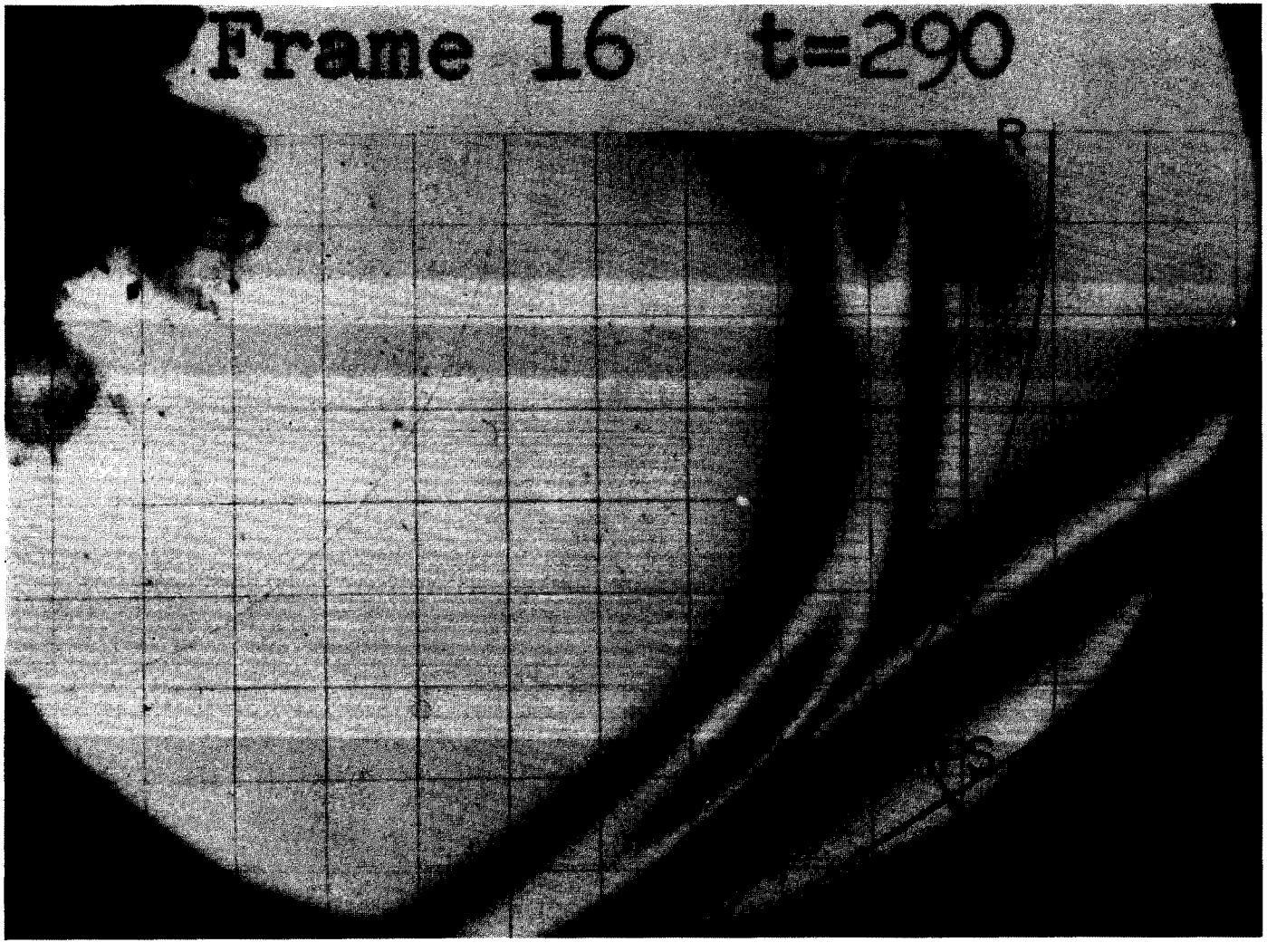

FIG. 7. Photoelastic representation of the Rayleigh wave.

4.2 *Comparison of theoretical and experimental results*

The results obtained for the boundary stress τ_{xx} as a function of position are shown in Figs. 8–11. These results for the boundary stresses are shown for four selected times during the dynamic event which include t equal to 60, 92, 139, and 208 μsec.

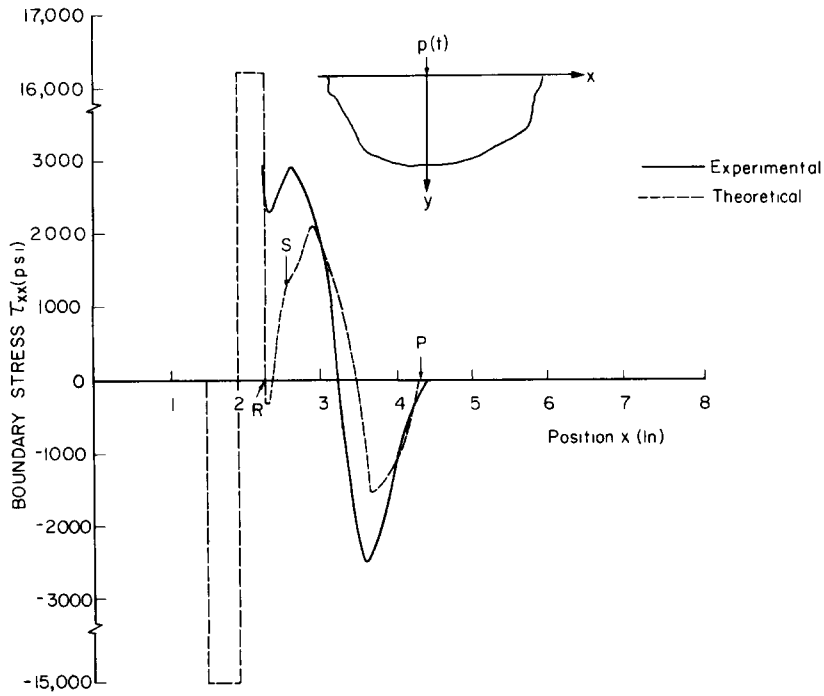

FIG. 8. Theoretical and experimental results for stress τ_{xx} at $t = 60$ μsec.

Superimposed theoretical and experimental results obtained at $t = 60$ μsec are shown in Fig. 8. The comparison shows that the arrival of the P wave front and the compressive P wave peak agree well. The decay of the compressive P stress and the subsequent build up of the tensile tail are also in close agreement although the experimental values of arrival times lag the theoretical values. The sharp increase in stress at the arrival of the Rayleigh front is also noted in both cases. Differences occur regarding predicted and measured amplitudes. The experimental values of the peaks of the P wave stresses are higher than the theoretical values. The sharp reduction in stress at the arrival of the S wave which is theoretically predicted is not totally obtained experimentally.

The theoretical and experimental results obtained at $t = 92$ μsec shown in Fig. 9 also indicate relatively good agreement. The experimental arrival times of the compressive and tensile peaks lag behind the theoretical predictions. The magnitudes of these peak values of the P wave agree very well since the theoretical and experimental results were scaled to match at this time. Again, the theoretically predicted compressive peak associated with the S wave was not experimentally observed. The arrival of the Rayleigh wave peaks

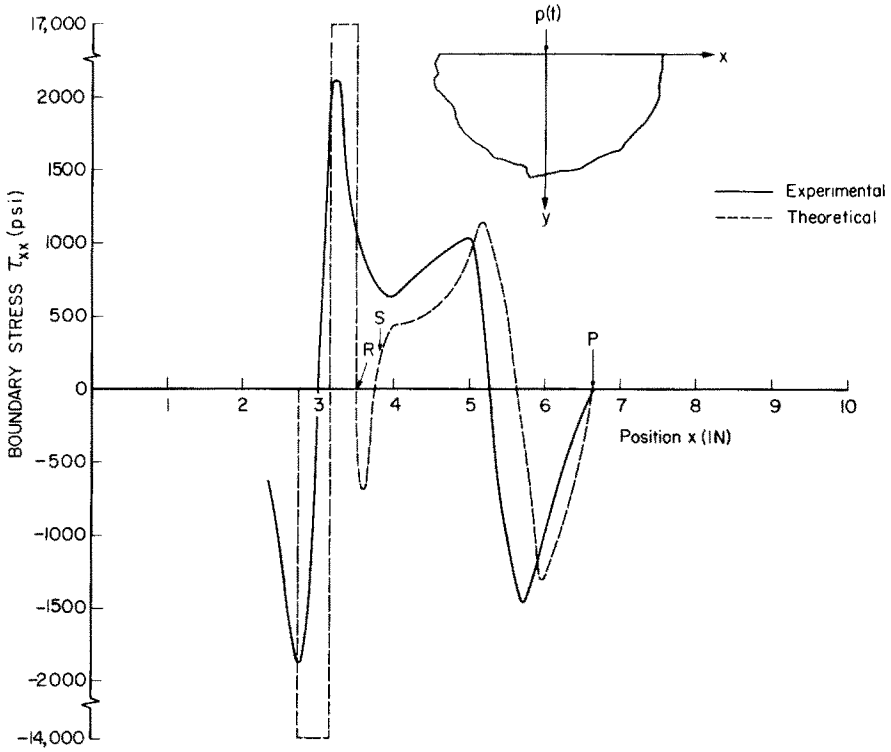

FIG. 9. Theoretical and experimental results for stress τ_{xx} at $t = 92\ \mu$sec.

compares well; however, the difference in amplitudes is very large with the experimental values smaller than the theoretical values by nearly an order of magnitude.

The theoretical and experimental results obtained at $t = 139\ \mu$sec shown in Fig. 10 are comparable with the previously described comparison. The experimental maximums for the P and R waves lag behind the theoretical predictions. The compressive pulse due to the S wave is not observed in the experiment, and an order of magnitude difference exists in the amplitude of the Rayleigh wave with the experimental results being the lower of the two reported values.

The final comparison presented in Fig. 11 for $t = 208\ \mu$sec shows an appreciable lag in the arrival times of the experimental peak values of the stresses. Also, the magnitudes of the experimental values of the maximum stresses have dropped below the theoretically predicted values. These results indicate a more rapid attenuation and spreading of the experimentally determined stresses in comparison with the theoretical predictions.

To further show the attenuation characteristics, the maximum values of the compressive and tensile stresses associated with the P wave are plotted in Fig. 12 at each position along the boundary. It is observed that the experimental magnitudes are greater close to the point of loading and that they decay more rapidly than predicted by theory. The theoretical values are larger for the compressive peak after it has traveled about 7 in., while for the tensile peak, the theoretical values become greater beyond 3·5 in. from the load.

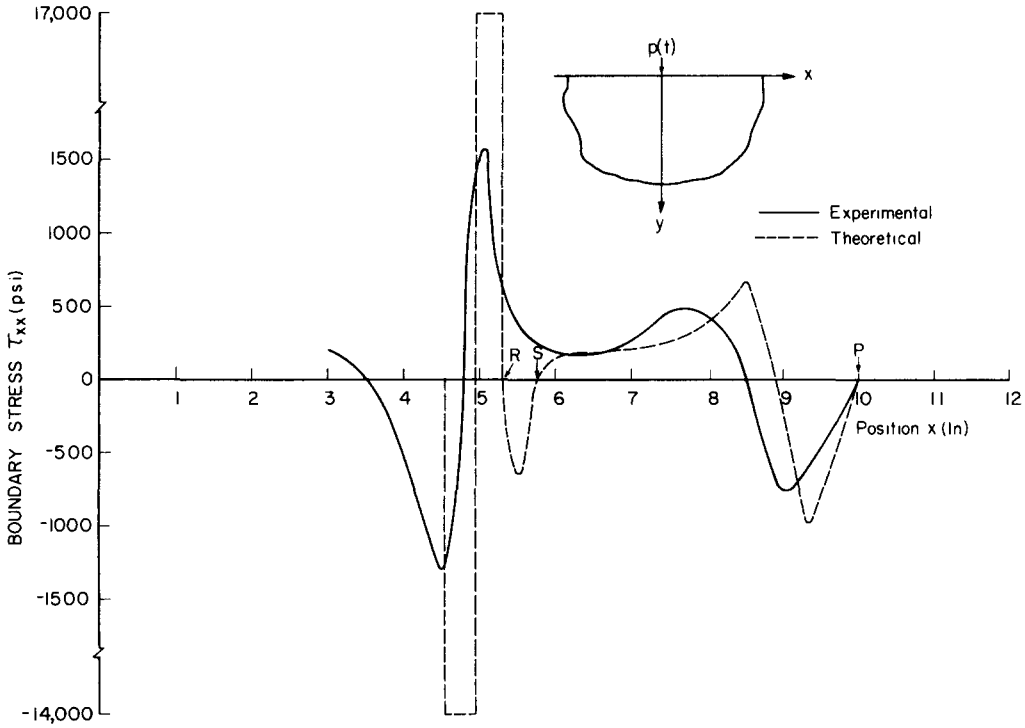

FIG. 10. Theoretical and experimental results for stress τ_{xx} at $t = 139$ μsec.

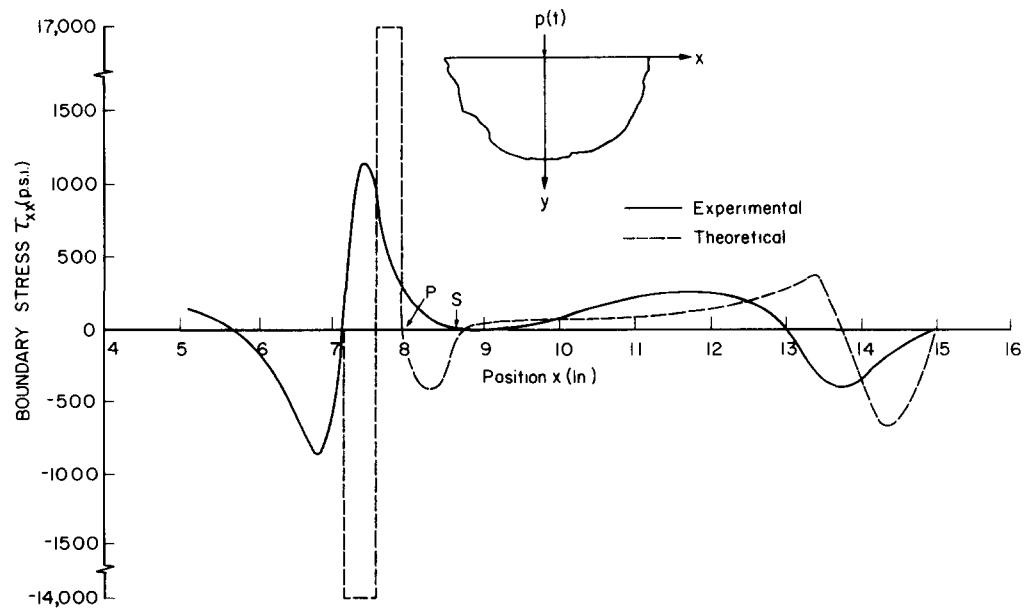

FIG. 11. Theoretical and experimental results for stress τ_{xx} at $t = 208$ μsec.

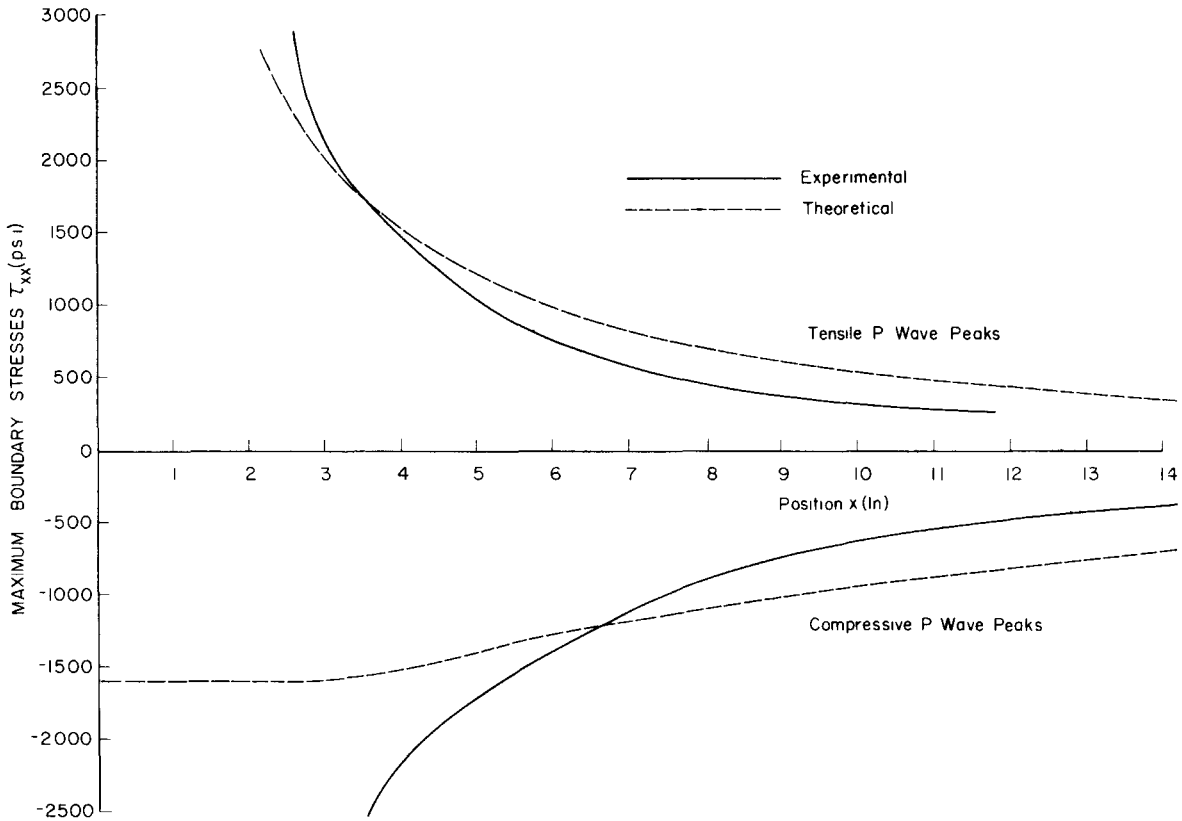

FIG. 12. Attenuation of maximum compressive and tensile stresses associated with the *P* wave.

Strikingly different behavior of the theoretical values of the peak compressive stress is found near the load. The theoretical two-dimensional solution predicts zero compressive stress parallel to the boundary directly under the load. Away from the load, a constant maximum value of compressive stress is maintained for a distance where effects generated only during the loading period have arrived. The constant loading rate is just enough to counteract the geometric attenuation of the outgoing P wave. After combined effects of the total loading pulse occur, the P wave compressive amplitude, decays as expected.

The attenuation of the Rayleigh wave stresses is presented in Fig. 13. The theoretical solution does not predict attenuation of the stresses associated with the Rayleigh wave; the experimental results clearly indicate a decay in amplitude with distance of propagation.

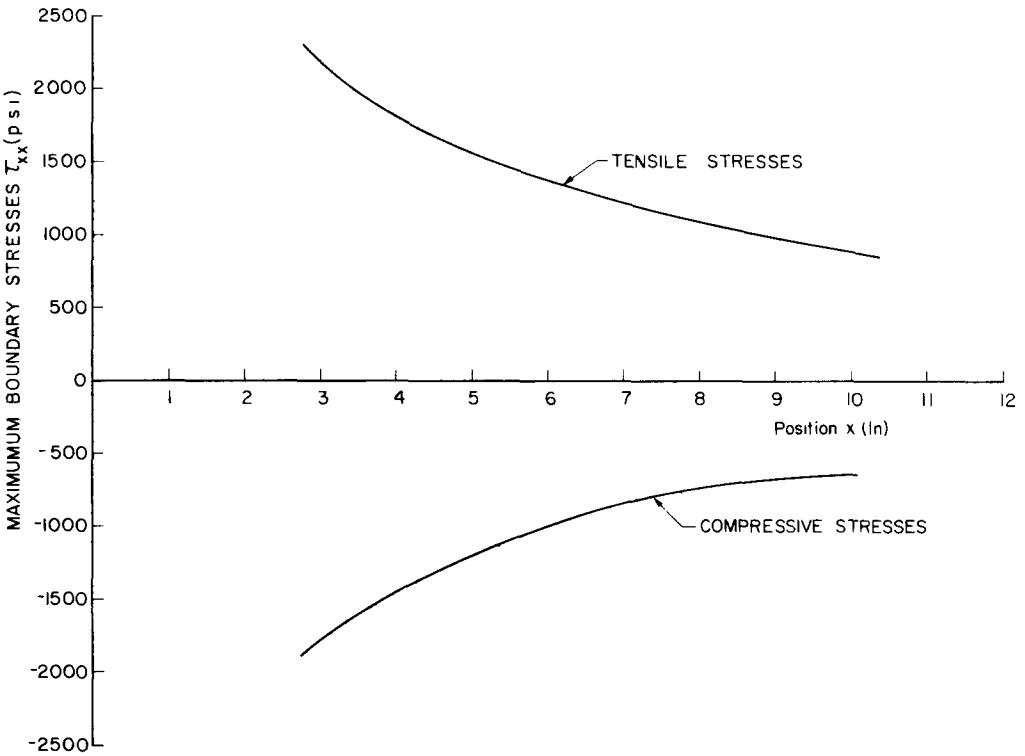

FIG. 13. Attenuation of maximum compressive and tensile stresses associated with the R wave.

5. DISCUSSION AND CONCLUSIONS

The propagation of stress waves in a thin semi-infinite plate with an explosive load acting on the boundary has been studied by the photoelastic method. Special attention is directed to observations of the wave pattern near the boundary; and numerical values of the non-zero principal stress along the boundary are calculated and compared to those obtained from an elastodynamic generalized plane stress solution.

Theoretical calculations of the principal stress along the free edge of the half-plate are based on the idealized two-dimensional model of a semi-infinite plane with a concentrated normal load whose magnitude varies with time in the form of a triangular pulse. For the

purpose of comparing the two results, the theoretical stress values associated with the leading P waves are adjusted to match approximately the corresponding photoelastic ones at a particular observation time. The agreement, then, of the two sets of results for all waves at the other observation times is considered good in that the overall features of the boundary stress variation are duplicated; and further, since discrepancies in the results can be attributed to differences in the experimental and theoretical models.

Effects of internal dissipation plus effects caused by the actual three-dimensional geometry, which introduces the phenomenon of dispersion are both neglected in the generalized plane stress analysis, and are believed to explain some of the discrepancies in the results. Both dissipation and dispersion cause the actual stress magnitudes to decay more rapidly while dispersion also causes the width of a pulse to increase as it propagates. Briefly, dispersion means that the velocity of a wave depends on the frequency components of the wave and it occurs in a plate from the interaction of the waves with the front and back surfaces of the plate. Dispersive effects become negligible as the characteristic wave lengths become large in comparison with the plate thickness. According to the theory of elastic wave propagation in plates [9], the generalized plane stress approximation is accurate if

$$\text{wave length} \gg \pi \times \text{plate thickness.}$$

A calculation of the predominant wave lengths in the frequency spectrum of the experimentally measured response of the P and R waves indicated the P wave length to be about equal to $\pi \times$ plate thickness, while the Rayleigh wave length is about $\frac{1}{2}$ that of the P wave. Thus, the effects of internal friction and dispersion appear to account for the greater rate of attenuation and spreading observed experimentally in propagation of P and R waves.

Another difference between the experimental and mathematical models, which is thought to explain the discrepancies in the P wave stress values close to the point of loading, is in the description of the loading. In the experiment, the explosive charge not only creates a net normal force, but also it produces components of force acting parallel to the boundary of the half-plane. The dynamic field due to this double tangential loading will decrease with distance more rapidly than the field caused by the normal force since, by symmetry, the net tangential force is zero. Thus, it is neglected in the theoretical analysis. (For example, in two-dimensional plane static problems, stresses decay with distance from a point force as $1/r$, but decay as $1/r^2$ from two equal but oppositely directed forces located close together.) It is found, however, that the experimentally obtained values of stress associated with the leading P waves become greater than the theoretical values as the observation station is taken closer to the point of loading. In fact, the theoretical peak compressive P wave stress along the boundary due to the normal force alone propagates with a nearly constant value during the period of loading and does not begin to decrease until the unloading cycle occurs. This is not found from the experimental data, but instead both the compressive and tensile peaks continually increase with decreasing distance from the boundary load. It is believed that these differences can be corrected by including in the theory the action of two equal and opposite tangential forces acting very close together, for they will produce initially large compressive stresses and will also increase the tensile stress pulse which follows.

It is believed that the striking differences in the experimentally and theoretically predicted S and R wave amplitudes can be attributed to the fracturing of the model in the neighborhood of the explosive charge. Large values of the compressive stress associated

with the P wave can be supported by the CR-39 and hence are propagated into the model. However, the tensile stresses in the tail of the P wave are large enough to produce localized fracturing. This fracturing relieves the load to a significant extent as much of the energy associated with the explosive charge is utilized in forming multiple fracture surfaces and in accelerating the debris particles. Thus, the magnitude of the subsequently formed S and R waves are also significantly decreased as experimentally observed. It appears that a more inclusive mathematical model is necessary to describe the observed results. This model should at the very least incorporate a bi-level forcing function.

It appears that the excellent agreement of static two-dimensional photoelastic results with the corresponding values obtained from a plane stress elastostatic analysis is very difficult to achieve for dynamic problems. There are several factors occuring in dynamic problems which are less pronounced or non-existent in static situations. Furthermore, these additional features are difficult to eliminate or control in an experiment and may add so much complexity to mathematical analysis as to make it impossible. Effects of dissipation, dispersion, and fracture as well as modeling the experimental loading function encountered in this problem should be considered typical. Nevertheless, a great deal of insight regarding the physical nature of complex dynamic problems can be gained by a combined theoretical and experimental approach.

Acknowledgements—The research work described herein was sponsored by the National Science Foundation. The authors would like to express their appreciation to Drs. John Ide and Michael Gaus for their support and encouragement.

REFERENCES

[1] W. M. Ewing, W. S. Jardetzky and F. Press, *Elastic Waves in Layered Media*. McGraw-Hill (1957).
[2] J. W. Sherwood, Elastic wave propagation in a semi-infinite solid medium. *Proc. phys. Soc., Lond.* **71**, 207 (1958).
[3] Y. C. Fung, *Foundations of Solid Mechanics*, pp. 214–225. Prentice-Hall (1965).
[4] J. C. Feder, R. A. Gibbons, J. T. Gilbert and E. I. Offenbacher, The study of the propagation of stress waves by photoelasticity. *Proc. Soc. exp. Stress Analysis* **14**, 109 (1956).
[5] J. W. Dally, A. J. Durelli and W. F. Riley, Photoelastic study of stress wave propagation in large plates. *Proc. Soc. exp. Stress Analysis* **17**, 33 (1959).
[6] C. Cranz and H. Schardin, Kinematographie auf ruhendem Film und mit extrem hoher Bildfrequenz. *Z. Phys.* **56**, 147 (1929).
[7] J. W. Dally and W. F. Riley, Stress Wave propagation in a half-plane due to transient point load. *Proc. 3rd Southeastern Conf. theo. appl. Mech.* To be published.
[8] A. B. J. Clark, Static and dynamic calibration of a photoelastic model material–CR-39. *Proc. Soc. exp. Stress Analysis* **14**, 195 (1956).
[9] R. D. Mindlin, An introduction to the mathematical theory of vibrations of elastic plates, U.S. Army Corp., Engineering Laboratories Monograph, Fort Monmouth, New Jersey (1955).

(*Received* 26 *July* 1966; *revised* 17 *October* 1966)

Résumé—Cette investigation traîte d'un demi-plan avec une charge de limite employant une analyse combinée théorique et expérimentale. L'approche théorique considère une plaque semi-infinie isotrope, parfaitement élastique avec une charge normale concentrée à la limite. Le modèle expérimental consiste en une grande feuille de résine de colombie CR-39 chargée d'un chargement d'azide de plomb dans une fosse semi-cylindrique sur le bord de la plaque. Les résultats de la tension de limite des analyses photoélastiques théoriques et dynamiques étaient comparés. La comparison a montré un accord pour les effets dus à l'onde P et des differences marquées mais explicables dans les résultats théoriques et expérimentaux associés aux ondes S et R. Il semble qu'une meilleure correlation entre les fonctions de chargement et les modèles expérimentaux et mathématiques est nécessaire afin d'améliorer l'accord.

Zusammenfassung—Diese Arbeit untersucht die Halbebene mit Grenzbelastung mittels kombinierter theoretischer und experimenteller Analyse. Die Theorie behandelt eine isotrope, vollkommen elastische Platte, die semiunendlich ist, und eine konzentrierte Grenzlast hat. Das Experimentalmodell bestand aus einer Kolumbiaharzplatte CR-39 die mit Bleiazid in einer halbylindrischen Vertiefung am Plattenrand belastet wurde. Die Resultate der Grenzspannungen aus theoretischen und Versuchsanalysen wurden verglichen. Diese Vergleiche zeigten Übereinstimmung für die Resultate der P Welle und nennenswerte aber unerklärte Unterschiede zwischen theoretischen und experimentellen Resultaten die mit den S and R Wellen zusammenhängen. Es scheint, dass eine bessere Beziehung der Belastungsfunktionen gefunden werden muss um die Übereinstimmung zu verbessern.

Абстракт—Это исследование рассматривает полуплоскость с граничной нагрузкой, применяя комбинированный теоретический и экспериментальный анализ. Теоретический подход касается изотропической, идеально-эластичной полубесконечной пластины с концентрированной нормальной нагрузкой на границе. Экспериментальная модель состоит из большого листа колумбийской (ниобиевой) смолы CR-39, загружённого зарядкой окиси свинца (азотоводородной соли свинца) в полуцилиндрической впадине на краю пластины. Сравнивались результаты граничного напряжения теоретических и динамических фотоупругих анализов. Сравнение показывает согласованность эффектов, обусловленную P волной и отмеченную, но обьяснимую разницу в теоретических и экспериментальных резулвтатах, связанных с S и R волнами. Из этого явствует, что, чтобы улучшить согласованность для экспериментальных и математических моделей, требуется лучшее соотношение между функциями загружения.